Cutoff rigidities, galactic cosmic ray flux, and heavy ion detections at Jupiter

Martin B. Enghoff[1], Jacob Svensmark[2,3], Heidi N. Becker[4], John L. Jørgensen[1], Stavros Kotsiaros[1], Matija Herceg[1], James W. Alexander[4], Meghan M. Florence[4], John E. P. Connerney[5]

[1]National Space Institute, Technical University of Denmark, Kongens Lyngby, Denmark
[2]Atmospheric, Oceanic and Planetary Physics, Department of Physics, University of Oxford, Oxford, UK
[3]Niels Bohr Institute, University of Copenhagen, Copenhagen, Denmark
[4]Jet Propulsion Laboratory, California Institute of Technology, Pasadena, California, USA
[5]Space Research Corporation, Annapolis, MD, USA

Key Points:

- A galactic cosmic ray cutoff rigidity map for Jupiter was made using the JRM33 model and the Geomagnetic Cutoff Rigidity Computer Program
- The flux of galactic cosmic ray protons into Jupiter's atmosphere was calculated based on BESS-Polar ii data
- Detections of heavy ions by Juno's SRU were investigated and used to estimate their equatorial pitch angles

Corresponding author: Martin B. Enghoff, `enghoff@space.dtu.dk`

Abstract

A map of vertical cutoff rigidities has been calculated for galactic cosmic ray (GCR) entry into the atmosphere of Jupiter at the 1 bar pressure radius (1 R_J = 71,492 km) using the JRM33 comprehensive model of Jupiter's magnetic field (based on 32 close flybys of Jupiter by the Juno satellite) along with a particle trajectory code (Geomagnetic Cutoff Rigidity Computer Program). The map was combined with measurements of the GCR proton flux at Earth, from the BESS-Polar ii campaign, to calculate a corresponding proton flux map at Jupiter. Additional cutoff rigidity maps were calculated for 1000 km above the 1 bar level, and for 1.41 R_J.

Furthermore, detections of heavy particles from Juno's Stellar Reference Unit were analyzed for their cutoff rigidities in multiple directions. Cutoff rigidities of 3.5-8.5 GV were found for the five detections furthest out making them possible GCR candidates. The majority of points, located below 1.6 R_J are not likely to be GCR. Assuming instead that they are trapped particles we have calculated upper and lower limits on their equatorial pitch angles, resulting in a range from 10.1° to 27.1°, which can help constraining Jupiter's energetic radiation.

Plain Language Summary

Using data of Jupiter's magnetic field, collected by the Juno satellite, we have calculated how galactic cosmic rays (energetic particles originating from supernovae) can enter into the atmososphere of Jupiter at different altitudes. This can aid our understanding of atmospheric phenomena on Jupiter and help in planning future missions to the planet.

One of Juno's instruments, the Stellar Reference Unit, has detected some peculiar signatures. Some of them probably are galactic cosmic rays that have hit the instrument. Most of them are probably not, but instead they could be particles trapped by the strong magnetic field of Jupiter. If so, they can help us understand the radiation belts of the planet. Using knowledge of the location of the detections as well as the magnetic field we calculate the so-called pitch angle of the detected particles. This angle is defined by the ratio between the motion of the particle perpendicular to the magnet field line and the motion parallel to the field line. The pitch angle is fundamental in constraining energetic radiation emanating from Jupiter's atmosphere.

1 Introduction

Galactic cosmic rays (GCRs), primarily consisting of protons, are ubiquitous throughout the solar system. The magnitude of the GCR flux is determined by the incoming amount and modulation by sources within the solar system itself. The incoming flux is primarily controlled by galactic sources such as supernova activity (Patrignani et al., 2016; Piazzoli et al., 2022) which varies on timescales of tens to hundreds of millions of years based on the movement of the solar system into and out of the spiral arms of the Milky Way (Shaviv, 2002) and on shorter timescales in case of nearby supernovae which happened, for instance, about 1.5 and 2.3 million years ago (Breitschwerdt et al., 2016). The flux is modulated by the solar wind, which operates with the characteristic 11-year solar cycle (Lockwood & Webber, 1996) but also with longer term variability on timescales of hundreds to thousands of years (Lundstedt et al., 2006). Within the solar system a GCR gradient of a few percent per AU has been detected using data from Voyager 1 and 2, Pioneer 10, and IMP 8 (Lockwood & Webber, 1984) and later using Cassini with ground based measurements (Roussos et al., 2020) as well as INTEGRAL and Rosetta (Honig et al., 2019).

Planets and other celestial bodies can be individually shielded against GCRs if they possess a magnetic field. The magnetic field of Earth is very well described by the International Geomagnetic Reference Field (Alken et al., 2021). It is therefore possible to calculate a map of cutoff rigidities for cosmic ray particles (Smart & Shea, 1994, 2005; Mertens et al., 2012), defined as the minimum rigidity (P in units of GV) required to penetrate the magnetic field and enter the atmosphere. P is defined as $P = pc/|q| = r_L B$, where c is the speed of light, p the particle momentum, q the charge, r_L the gyroradius, and B the magnetic field strength. Particles with the same rigidity thus also have the same gyroradius. For energetic (GeV) protons the rigidity (in GV) is nearly equal to the energy (in GeV, e.g. a 10 GV rigidity proton has an energy of 9.1 GeV). The lower the numeric value of the energy is, the larger the discrepancy between the energy and rigidity becomes. Sufficiently energetic particles entering a planetary atmosphere can initiate air showers, the formation of radioactive elements, and cause atmospheric ionization (Usoskin & Kovaltsov, 2006). On Earth ionization from GCRs have been linked to various atmospheric phenomena such as cloud formation (Svensmark et al., 2021) via the formation of stable molecular clusters (Enghoff et al., 2008; Lovejoy et al., 2004) able to serve as cloud condensation nuclei (Svensmark et al., 2013).

The magnetic field of Jupiter is described in great detail by the JRM33 model (J. E. P. Connerney et al., 2022) using data from the still ongoing Juno mission (S. J. Bolton et al., 2017; J. E. P. Connerney et al., 2017) and has been measured previously by a variety of missions (J. E. P. Connerney et al., 1998; Hess et al., 2011; J. Connerney, 2015; Ridley & Holme, 2016). Jupiter exhibits interesting atmospheric phenomena at high latitudes (Romani et al., 2008) where the galactic cosmic ray flux is typically highest for planets with a strong magnetic dipole aligned with the axis of rotation (Usoskin & Kovaltsov, 2006) and several high energy particle events have been detected by Juno's Stellar Reference Unit star camera at close range to Jupiter (Becker et al., 2021). Jupiter's atmosphere has also been suggested as a detector of ultra-high-energy cosmic rays (Rimmer et al., 2014) although the feasibility is limited by geometric aperture size and detectable energies (Bray & Nelles, 2016). Cutoff rigidities for Jupiter have previously been estimated for large ($> 10\ R_J$) distances (Selesnick, 2002) using a dipole approximation of the magnetic field. Jupiter's ability to trap secondary GCRs via the Cosmic Ray Albedo Neutron Decay (CRAND) process also depends on which GCRs can gain access to the radiation belts of the planet (Roussos et al., 2021). Furthermore, trapped particles contribute to the synchrotron emission of Jupiter (S. Bolton et al., 2002; Santos-Costa & Bolton, 2008).

Jupiter's radiation belts consist of trapped energetic heavy ions up to sulfur which is the most abundant ion along with oxygen. These have previously been detected by the Galileo probe (Fischer et al., 1996) and to some degree Pioneer 11 (Pyle et al., 1983). Their origin is discussed by Roussos et al. (2022) while Becker et al. (2021) compares the observations with those from Juno.

In this work we use a modified version of the Geomagnetic Cutoff Rigidity Computer Program by Smart and Shea (2001), a particle trajectory program made for Earth's magnetic field, to calculate galactic cosmic ray vertical cutoff rigidity maps for Jupiter at altitudes relevant for GCR shower formation and further out. These maps are then folded with the solar minimum GCR spectrum measured by the BESS-Polar ii Antarctic mission (Abe et al., 2016) to calculate a map of total proton flux at Jupiter. Furthermore, we investigate if high energy heavy particles detected by Juno (Becker et al., 2021) could be direct hits by GCRs by calculating detailed cutoff rigidity skyview maps at the locations of the detections. Finally, we estimate the equatorial pitch angles of the particles least likely to be GCRs, assuming that they are instead trapped particles.

2 Methods

2.1 Magnetic fields

For describing Jupiter's magnetic field we use the JRM33 model compiled from 32 polar orbits of Juno's prime mission going as close as ~ 1.05 R_J at perijove (PJ). The orbits were 53 days long and reached 113 R_J at apojove. The mission was designed to make a closely spaced longitude grid, covering the planet. Since the end of the prime mission in 2021 an extended mission has started, scheduled for an additional 42 orbits, with decreasing period. Further orbital information can be found in J. E. P. Connerney et al. (2022).

Although the model describes the field with 30 degrees and orders of Legendre functions we only employ the first 12 since little additional detail is gained from adding higher orders (4 % standard deviation between a 1x1 degree grid a 1 R_J and order 11 and 12) and the program used to calculate cosmic ray trajectories is limited to 12 orders without further modification (see Sect. 2.2). We choose to ignore the influence of the magnetodisk, although it has been shown to affect rigidities beyond 10 R_J (Selesnick, 2002).

2.2 GCR cutoff rigidities

The Geomagnetic Cutoff Rigidity Computer Program by Smart and Shea (2001) is used to calculate cutoff rigidities. The program uses the spherical harmonic approximations of the magnetic fields to calculate trajectories of GCRs entering the planetary atmosphere at different geographic locations. It is impractical to calculate approaching trajectories of the predominantly positively charged GCRs as the location where they hit the planetary atmosphere cannot be known in advance. Instead the program calculates the trajectory of a negatively charged particle leaving the planetary atmosphere. A trajectory is allowed if it can escape the magnetic field (i.e. reach the magnetopause).

The program was originally developed for Earth and we have thus modified it for use with Jupiter. On Earth the boundary for entering the atmosphere is traditionally set at 20 km above the reference ellipsoid (Smart et al., 2006; Vargas & Valdés-Galicia, 2011) since this is where the atmosphere is dense enough for typical air showers of secondary particles to begin. This height has been changed to that of a similar pressure in the atmosphere of Jupiter (67.5 km above the 1 bar pressure level of 71,492 km (J. E. P. Connerney et al., 2022)), using scale heights of 8 km for Earth and 27 km for Jupiter to calculate where the pressure at Jupiter is equal to that at 20 km on Earth. Furthermore the program requires the planetary radii both at the equator, at the poles, and the average to determine the reference ellipsoid. For a full list of program parameters altered see Tab. A1 in the appendix. Lastly the magnetic field parameters mentioned in Sect. 2.1 are read in to the program.

In reality the GCR could have any angle of approach but to reduce the amount of computation needed we focus on vertical approaches, so unless otherwise mentioned the cutoff rigidities reported here are vertical cutoff rigidities. Cutoff rigidities are then scanned from a user-defined upper limit, at regular intervals (unless otherwise noted we used 0.9 GV except for above/below 80N/80S where 0.05 GV was used). For each rigidity the trajectory is calculated. If the trajectory re-enters the atmosphere (i.e. it is unable to escape the magnetic field) it is deemed forbidden, but if it reaches a pre-determined distance determined by the location of the planetary magnetospause (set to 80 R_J, although the exact location varies (Selesnick, 2002)) the trajectory is deemed allowed. Above a certain rigidity all trajectories will be allowed and below another rigidity all trajectories will be forbidden. Between these limits there is a range of rigidities where there are both allowed and forbidden trajectories due to the complexity of the magnetic fields and their interaction with the gyroradii at specific rigidities. This range is called the penum-

164 bra. The program determines, where possible, both the start and end of the penumbra
165 at each location, and the cutoff rigidity is then the average between the two.

2.3 GCR flux

167 The galactic cosmic ray spectrum spans a very wide range of energies from a few
168 MeV to hundreds of TeV (Patrignani et al., 2016; Piazzoli et al., 2022). Energies below
169 10 GeV are modulated by solar activity, above this energy the spectrum follows a sim-
170 ple power law:

$$I_N(\text{E/nucl}) \approx 1.8 \times 10^4 (E/1 \text{ GeV/nucl})^{-\alpha} \text{ nucleons } (\text{m}^2 \text{ s sr GeV})^{-1} \ , \qquad (1)$$

172 where α is 2.7. About 79% of the nucleons are protons and most of the rest ($\approx 70\%$) make
173 up helium nuclei. This ratio is almost constant for the energies where Eq. 1 is valid, at
174 lower energies the ratio changes depending on the units used (e.g. GeV/nucleon or GV)
175 and on solar modulation (Abe et al., 2016; Patrignani et al., 2016).

176 For this calculation we are focusing on protons and thus energy per nucleon equates
177 total energy. The data we use for calculating the flux of GCRs into Jupiter's atmosphere
178 are BESS-Polar ii balloon measurements (Abe et al., 2016). These measurements were
179 performed at Antarctica where the geomagnetic cutoff rigidity is minimal, allowing nearly
180 all GCR to enter the atmosphere. The measurements were performed at solar minimum
181 where the solar modulation of the GCR spectrum is at its minimum.

182 To calculate the flux the BESS data were fitted with 4 different functions describ-
183 ing the complete measured spectrum. The lowest energies, which are most affected by
184 solar modulation, have been fitted with 4 and 5 order polynomials while the higher en-
185 ergies can be fitted by power laws. The fit used for energies above 20.5 GeV can be ex-
186 tended beyond BESS data as the power law dependency in this regions is well known
187 (Patrignani et al., 2016), as shown in Eq. 1. Data and fits are shown in Fig. 1. To find
188 the total flux for each location the cutoff rigidity (P, in GV) is first converted to kinetic
189 energy (GeV) using (Caballero-Lopez & Moraal, 2004):

$$E(\text{GeV/nucleon}) = \sqrt{(E_0)^2 \ + \ (n_z/n_a)^2 (P(GV))^2} - E_0 \ , \qquad (2)$$

191 where n_z is the charge number, n_a the mass number, and E_0 is the proton rest energy.
192 Note that the equation gives the kinetic energy per nucleon, but since we are concerned
193 with protons this is equal to the kinetic energy.

194 This cutoff energy is then used as input to integrate the relevant parts of Fig. 1.
195 The upper limit of the integral is set to 100 TeV, where the power law of Eq. 1 is still
196 valid. Above these energies the flux is extremely low and does not contribute significantly
197 to the total flux. The BESS measurements are performed at Earth, but there is a radial
198 GCR gradient in the solar system. Lockwood and Webber (1984) measured it to be about
199 3% per AU, but excluded regions below 6 AU. Roussos et al. (2020) extended this range
200 down to 1 AU and found a gradient varying between 2 and 4%, depending on solar ac-
201 tivity, while Honig et al. (2019) found a gradient of 2.96% per AU between 1 and 4.5 AU.
202 Additionally there is a latitudinal gradient in the GCR flux (Giesler & Heber, 2016; Owens
203 et al., 2020) which we are not concerned with, as Jupiter is very close to the ecliptic plane.
204 We thus use 3% per AU as an average gradient, while noting that both Sun to Jupiter
205 distance and the gradient itself varies in time. The average distance between Earth and
206 Jupiter is 715 million km (4.78 AU) with a variation between 588 and 968 million km
207 (3.9 and 6.5 AU). We have thus increased the proton flux by 14.3% (4.78 AU x 3 % per
208 AU).

2.4 Heavy ion detections

210 Juno's Stellar Reference Unit (SRU) star camera, part of the Radiation Monitor-
211 ing Investigation (Becker et al., 2017), recorded 118 events during Juno's first 21 PJs that
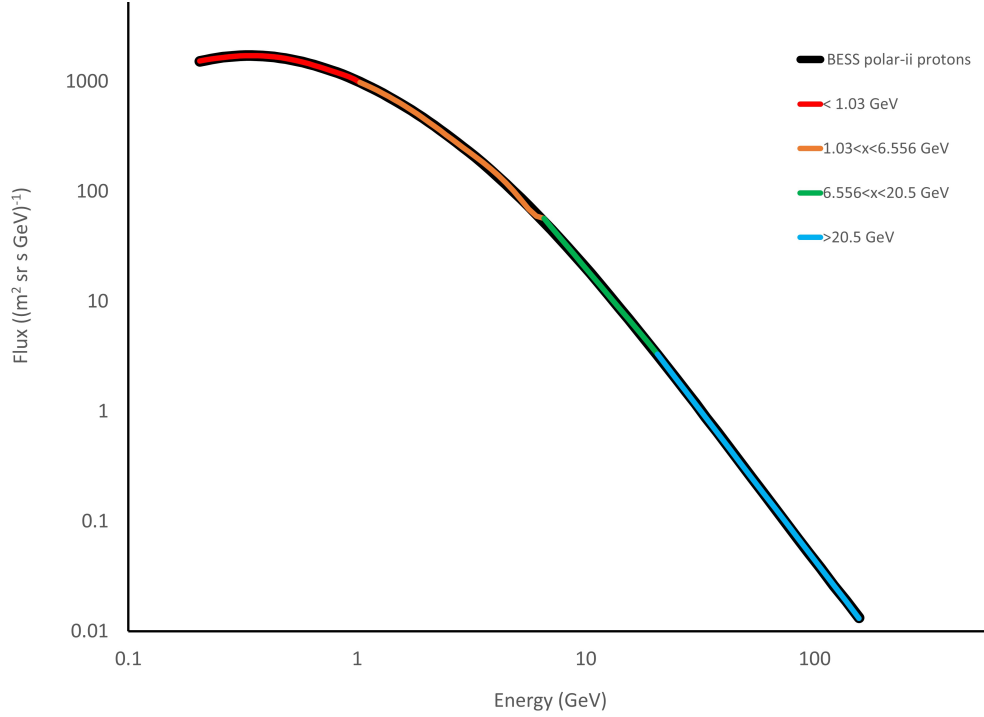
Figure 1: Proton flux spectrum as a function of kinetic energy, measured by BESS-Polar ii at the Antarctic during solar minimum (black line) and fits to 4 segments of the data (coloured lines).

were classified by Becker et al. (2021) as heavy ($2 \leq Z \leq 8$) ions of uncertain origin, with possible contributions from species as heavy as sulfur (Becker et al., 2021). Since then Juno has completed additional orbits and in this paper we present further suspected heavy ion detections for the following 21 PJs, thus covering PJ 1-42 (see Sect. 5 for data availability). As in Becker et al. (2021) we focus our analysis on images containing signatures with > 3000 DN (analog-to-digital data number) per pixel. A table of parameters for these additional detections can be found in the Supporting material.

The detections were made by analyzing image data collected by the CCDs of the SRU. The CCDs are strongly shielded but can be penetrated by energetic ions that leave a characteristic sharp and bright signature (Becker et al., 2017, 2021). Instrument characteristics of the SRU constrain upper and lower bounds for the energy and thus rigidity of the particles capable of producing the detected signal (for elements $Z \geq 6$ signal assessment were limited to up to ~ 10 GeV/nucleon) while the cutoff rigidity also sets a lower bound. Becker et al. (2021) states a cutoff rigidity of about 900 GV for the observation with the lowermost L-shell. While elements up to sulfur were considered, only $2 \leq Z \leq 8$ can explain the full range of the detected signals and since the highest allowed assessed rigidity for singly charged oxygen is 174 GV, cosmic rays are very unlikely as a potential source. Even if the highest allowed rigidity is above 174 GV, very few heavy GCR exist above 900 GV (corresponding to ~ 7200 GeV for fully charged oxygen) due to the powerlaw dependence on energy (as seen in Fig. 1).

3 Results and Discussion

3.1 Cutoff rigidity and proton flux maps

The cutoff rigidity for Jupiter at 67.5 km above the 1 bar ($1 R_J$) level is shown in Fig. 2 along with the corresponding allowed proton flux. The total magnetic field (at $1 R_J$) is plotted as contour lines on top. As for a dipole field the cutoff rigidity is highest close to the equator but the shape of the cutoff rigidity has a meandering pattern which seems to be caused by the strong magnetic region at around 50N and 200E and also by the Great Blue Spot (located just below the Equator at ∼270 E) (Moore et al., 2018). On one side of the Great Blue Spot the rigidity is high while on the other it is low, like the GCRs are bent around the spot. In this sense the Great Blue Spot appears to function like a dipole, guiding the GCRs in on one side while heavily shielding them on the other.

The proton flux map shows a pattern similar to that of the cutoff rigidity, but reversed. The shape of the cutoff rigidity map along with the GCR spectrum (as seen in Fig. 1) results in many orders of magnitudes difference in proton flux between the equatorial region and the poles. The meandering pattern of the rigidity map and particularly the anomaly of the Great Blue Spot complicates this pattern as Fig. 2 (right) reveals an enhanced proton flux around the south eastern edge of the Great Blue Spot. Heavier elements will follow a similar pattern as the proton pattern. The map gives an idea of how much energy is deposited by GCRs, which can be useful both for interpreting atmospheric phenomena and for future mission planning. The highest flux is found in the polar regions, as in dipolar fields. However, the meandering pattern of the cut-off rigidity also draws in an increased flux towards the Great Blue Spot and the magnetic maximum at 45^oN, 210° longitude.

A similar calculation was made for the cutoff rigidity at 1000 km above the 1 bar level to illustrate the altitude dependence. The result is shown in Appendix B - the shape and magnitude of cutoff rigidity is very similar to what is shown in Fig. 2.

To better understand the shape of the cutoff rigidity Fig. 3 shows the cutoff rigidity along with contours of 6 different components of the magnetic field and the magnetic equator. The shape of the cutoff rigidity follows the magnetic equator quite well and it appears that the curving around the Great Blue Spot is bending around a strong vertical (Z) field where there also are opposing maxima and minima in both the X and Y component of the magnetic field.

Confirming these calculations is probably not possible with the Juno instrumentation. The dedicated particle detectors, JEDI (Mauk et al., 2017) and JADE (McComas et al., 2017) are designed for lower (MeV and keV, respectively) energies. While the SRU cameras can detect energetic ions, as described below, it is not designed for discriminating the range of proton energies (> 1 GeV) considered here, as the stopping power of protons in silicon does not vary sufficiently. Similarly, the cameras for the MAG investigation (J. E. P. Connerney et al., 2017) are able to detect high energy protons but they also cannot discriminate and their signals are dominated by electrons. Electrons will also be a challenge for upcoming missions such as Europa Clipper's RadMon system (Meitzler et al., 2023) and JUICE's RADEM (Pinto et al., 2020) which has a separate proton detector and ion heavy ion detector although for sub GeV energies while Pix.PAN - an instrument proposed for future missions - expect to detect protons up to a few GeV (Hulsman et al., 2023). In order to fully test the calculations dedicated particle detectors capable of measuring different energy bands up to several orders of magnitude of GeV levels would be required. This is found on missions that have been used to measure the GCR flux, such as described by Honig et al. (2019); Roussos et al. (2020).
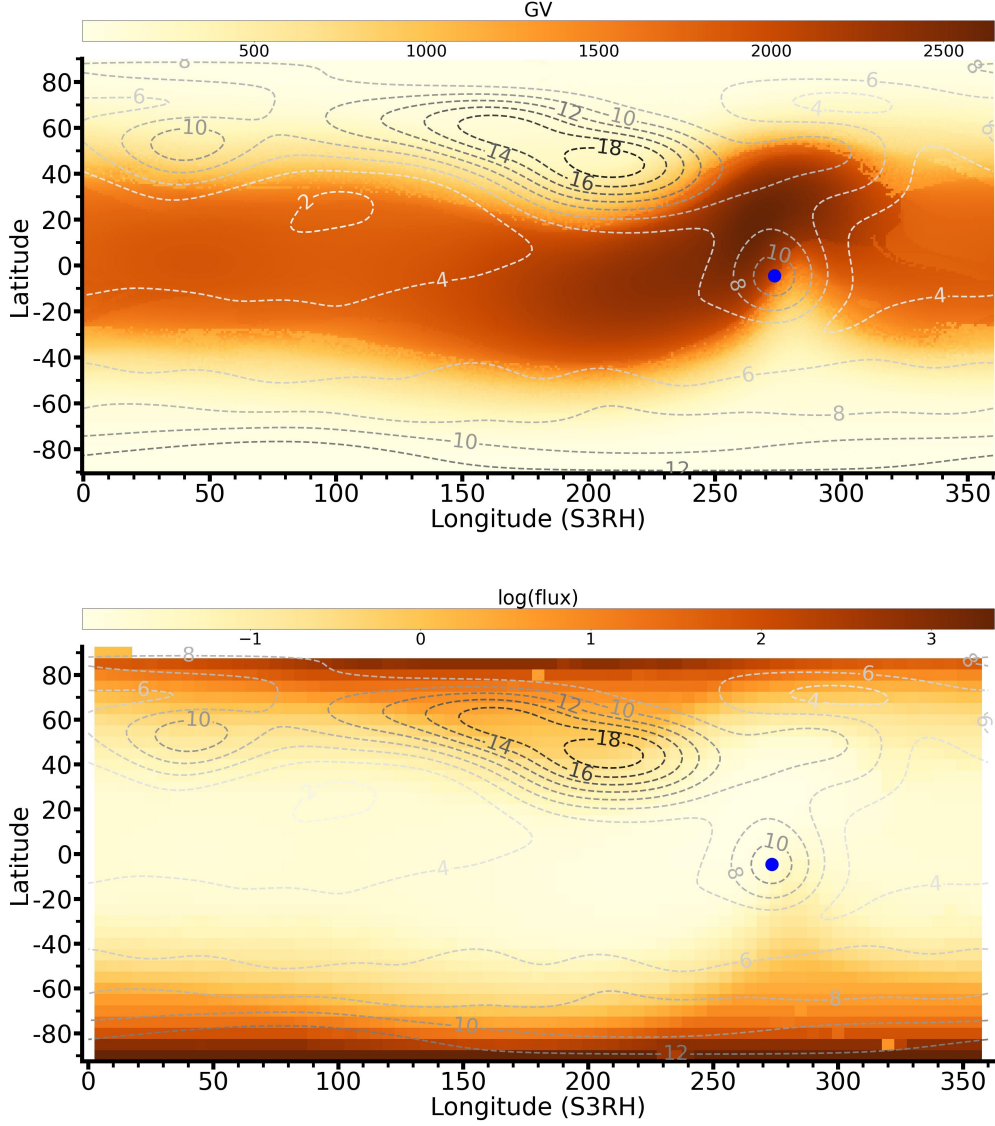
Figure 2: Top: The vertical cutoff rigidity map (in GV) of Jupiter at 1x1 degree spatial resolution. The average relative value between the start and end of the penumbra is 1.18 and the median is 1.08. The total intensity of the magnetic field (in Gauss) is overplotted as greyscale contour lines. The center of the Great Blue Spot is shown as a blue dot. Both the magnetic field and rigidities are calculated using 12 orders and degrees of Legendre functions. Bottom: The corresponding allowed GCR proton flux (in $(m^2 \ sr \ s)^{-1}$).
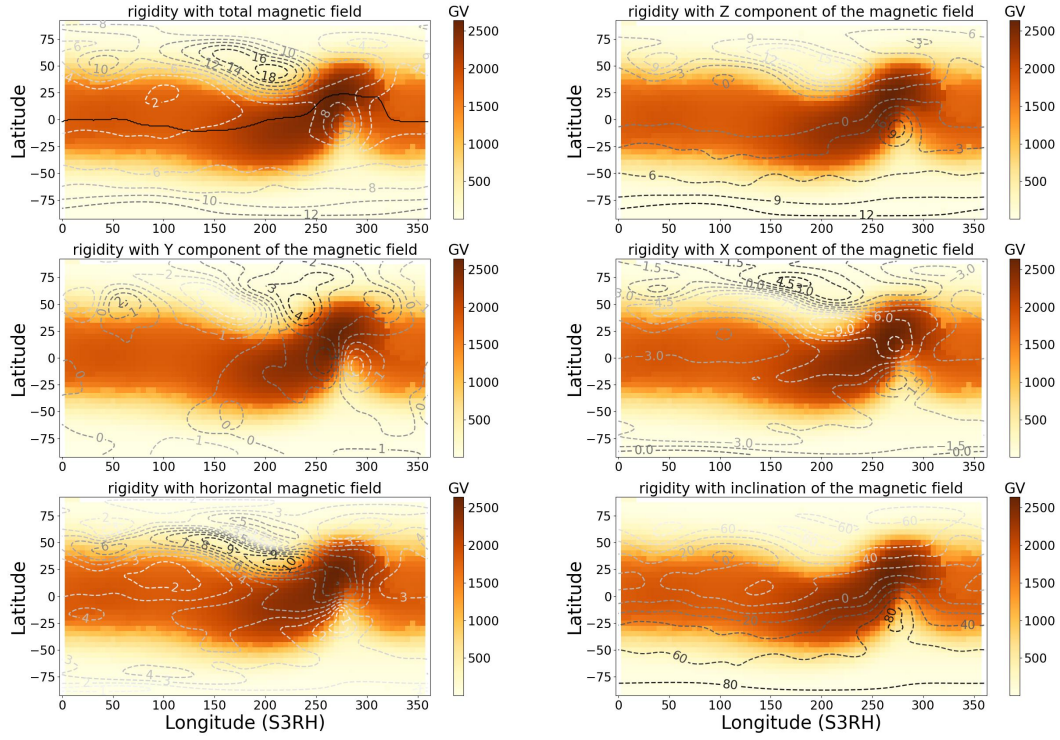
Figure 3: The cutoff rigidity map at 1 R$_J$ in 5x5 degrees spatial resolution, shown with 6 different components of the magnetic field in greyscale contour lines (total field, Z, Y, X and horizontal in Gauss and inclination in degrees). The dark black line (upper left figure) shows the magnetic equator, defined as the minimum in the magnetic inclination (between 25S and 25N to exclude the minimum at 40N 105E).

3.2 Heavy ion detections

In the following section we investigate the detections of heavy ions described in Sect. 2.4. Most of these are found close to the range of distances reported in Becker et al. (2021) (1.12-1.41 R_J) but a number of detections located much further out (from 1.95 to 15.5 R_J) have also been made and these are more likely to be GCRs. Note that the location of the detections, primarily within the Amalthea Ring, corresponds to where the Galileo Probe also detected intense heavy ion flux (Becker et al., 2021).

We have here calculated cutoff rigidities for the locations of the observations. A map of the cutoff rigidity at 1.41 R_J along with the locations of the observations of high energy particles and other details is shown in Fig. 4. The distance of 1.41 R_J is selected to be representative of most of the detections which are found to be at 1.11 $R_J \leq d \leq$ 1.57 R_J. All the observations are located on the edge of the high-cutoff rigidity areas except those which are detected further out than 1.6 R_J. As pointed out in Becker et al. (2021) different angles of approach can have different and even lower cutoff rigidities. To investigate this we calculate skyview cutoff rigidity maps for the locations of the detections. A full range of azimuthal angles of approach and zenith angles down to 75° have been investigated. For a simple dipole field an east-west asymmetry is expected based on traditional Störmer theory (Smart & Shea, 1994) and for a planet like Jupiter where the magnetic north is to the planetary north a lower cutoff rigidity is found for particles arriving from an eastward direction (Cooper & Simpson, 1980). However, Jupiter's magnetic field is more complicated than the dipole so there should be deviations from the simpler solution.

Figure 5 shows the cutoff rigidity as a function of zenith and azimuth angles at the location for one of the two detections made at 1.41 R_J and the detection found the furthest out, at 15.2 R_J. For the detection at 1.41 R_J northeastern directions are generally favored while northwest and southeast are the most heavily shielded. This is a more complex shape than predicted by Störmer theory. A simpler pattern is seen for the detection at 15.2 R_J, where the magnetic field more closely resembles a dipole. The lowest calculated cutoff rigidity for the detection at 1.41 R_J is found to be 456.5 GV at 15° zenith and 115° azimuth. The penumbra goes even deeper, down to 410 GV at 5° zenith and 0° azimuth. The penumbra might allow other specific rigidities as well, which were not found due to the 1 GV resolution. For the vertical approach a cutoff rigidity of 521.5 GV was found. As a test of whether 1.41 R_J is representative of the range of the observations (1.11-1.57 R_J) minimum and vertical cutoff rigidities were found for the same coordinates but at ranges of 1.11 and 1.57 R_J with results of 710.5 (856.5) GV and 363.5 (425.5 GV) for the minimum (vertical) cutoff rigidity. Both are within a factor of 2 of the 1.41 R_J value. Cutoff rigidities were also found for the other observation at 1.41 R_J (at 41.7S, 94.7E) with similar results, where the lowest calculated cutoff rigidity was 375.5 GV and a penumbra going down to 332 GV. While the cutoff rigidities found here are lower than that estimated by Becker et al. (2021) they are still quite high and the flux of GCRs at those rigidities is low.

Estimating the probability that the detections could be due to GCRs requires some assumptions. Using the detection depicted in Fig. 5A the minimum rigidity is 456.5 GV or 455.6 GeV. where the integrated proton flux (from eq. 1) is 0.32 nucleons $(m^2 \text{ s sr})^{-1}$. The area of detection of the SRU is of the order 1 cm^2 and assuming minimum cutoff rigidity in all directions (best case scenario) we get about 0.0004 protons s^{-1}. However, protons and all other elements up to carbon are ruled out (Becker et al., 2021) and the carbon flux is about 100 times lower than that of protons at equal energies (Patrignani et al., 2016). The effective time for detection can be constrained by looking at the total time where Juno is both within the latitude band of the observations (23.8 to 45.3^oS) and within the altitude band (1.11 to 1.57 R_J) which is 13 minutes. For all PJs this effective time for detection varies between 9 and 14 minutes for the southern detections. For the northern detections the effective time of detection, based on the same altitude
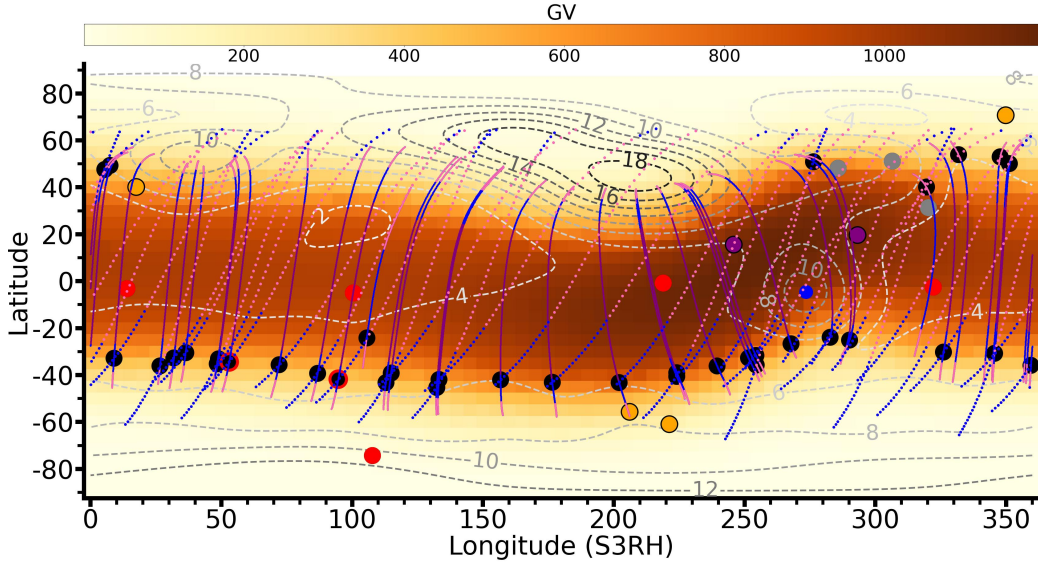
Figure 4: The vertical cutoff rigidity map (in GV) at 1.41 R$_J$. Black dots mark locations of the observations at d $\leq$1.6 R$_J$, those with red outline being the two observations directly at 1.41 R$_J$. Orange dots with black outline are detections at 1.6 R$_J < d < 3.22$ R$_J$, purple dots w. black outline observations at 6.09 and 6.14 R$_J$, grey dots are suspected proton overlaps, and red dots are suspected GCR events (with d > 3.6 R$_J$). Dashed greyscale lines show the contours of the magnetic field at 1 R$_J$. Fully drawn lines are the magnetic field lines which intersect with the observations while the dotted lines show the path of Juno during the orbit with the observation: Colors of orbits and field lines refer to the distance with pink: r$\leq$1.2 R$_J$, blue: r=1.2-1.6 R$_J$, purple: r$\geq$1.6 R$_J$.

band and latitudes from 40.2 to 53.9°N, is up to 6 minutes, with 0 minutes for PJs 34+. The northern detections are further limited by the shape of the field lines which terminate at lower latitudes around the magnetic anomalies (see Sect. 3.2.1), whereas the magnetic field on the southern hemisphere is more even.

So, although unlikely based on the above, a few detections could be due to GCRs by chance. However, the amount of detections and their consistent pattern makes another explanation more likely.

On the other hand the detection at 15.2 R$_J$ has a minimum rigidity of 5.5 GV at 75° zenith and 90° azimuth, with a vertical cutoff rigidity of 8.5 GV. The minimum rigidity in the penumbra is 5.0 GV. This is in the region of high GCR flux, as seen in Fig. 1. Four other detections at d=3.63, 13.8, 15.5, and 14.3 R$_J$ have been suspected to be caused by GCRs and the lowest found cutoff rigidity for these are 3.5, 7.5, 6.5, and 7.5 GV. These are in the range of allowed rigidities for all elements heavier than He for singly charged particles and for C and up for fully charged particles (see Supporting material of Becker et al. (2021)). The corresponding energy range for fully charged carbon is $\sim$ 13 − 30 GeV and the flux of carbon is 2-3 orders of magnitude below that of protons (Patrignani et al., 2016) (see Fig. 1). Two detections at 6.09 and 6.14 R$_J$ have minimum cutoff rigidities of 37.5 and 38.5 GV, making them less likely to be GCRs (about 210-220 GeV for fully charged carbon). Four detections at distances between 1.69 and 3.22 R$_J$ have minimum cutoff rigidities of 53-142.5 GV making a GCR origin even less likely, but not impossible. Galileo also found heavy ions at larger distances, with a peak just beyond Io at M-shells 6-8 (Roussos et al., 2022) further reinforcing our hypothesis that these heavy ion detections made by the SRU are not GCRs and indicating that they could be of local origin.

3.2.1 Pitch angles

Pitch angles of particles in Jupiter's radiation belts have been investigated since the detection of radio waves from Jupiter (Burke, BF and Franklin, KL, 1955) by e.g. Roberts (1976) who inferred pitch angles from radio observations and Moeckel et al. (2019) who used CASSINI data. The pitch angle is a useful parameter for modelling the synchrotron radiation around Jupiter (S. Bolton et al., 2001; Santos-Costa & Bolton, 2008; Levin et al., 2001; Nénon et al., 2017).

If most of the detections recorded by the SRU cannot be explained by direct hits of GCR then they could be due to trapped particles, as suggested by Becker et al. (2021). For all detections at distances of 1.6 R$_j$ and below, which are the least likely to be GCRs, Juno was in a narrow range of M-shells (1.5-2.39 for the observations shown in Fig. 4 excluding the detection at 24S, 106E which appears to be out of family). Furthermore the detections were in quite narrow latitude bands as well (40.2N-53.9N and 23.8-45.3S) associated with the synchrotron emission region. Trapped particles would also explain the pattern of the black points in Fig. 4. In the region between the southern and northern areas of detection Juno is flying too low to interact with the drift shell, and any further north/south brings Juno too high. This can be gleaned by the orbits and field lines shown in Fig.4 where the orbits dip low between the points of detection and then go upwards, while the field lines follow the opposite pattern. This can also explain the lack of detections in most of the northern hemisphere. Due to the altitude profile of the orbits compared to the relevant field lines they only interact at low altitudes, possibly below the mirror points, except at the west- and eastmost longitudes where detections are also found.

Assuming, as also concluded in Becker et al. (2021), that the particles are trapped in a stable drift shell, they are relevant for understanding Jupiter's synchrotron emissions (S. Bolton et al., 2002; Santos-Costa & Bolton, 2008). While not energetic enough to contribute directly to the synchrotron emission, investigating the particles' equato-

Table 1: Equatorial pitch angles

Method	Angle (mean)	Angle (std. deviation)
λ_m, mp = location of detection	<26.0/21.8/27.1°	5.60/5.51/5.10
B_{eq}/B_m, mp = location of detection	<25.7/23.6/26.3°	3.44/4.63/2.85
λ_m, mp = north field line end	>12.7/15.3/12.1°	4.57/4.47/4.37
λ_m, mp = south field line end	>14.7/12.9/15.1°	5.65/5.13/5.68
B_{eq}/B_m, mp = north field line end	>11.1/15.6/10.1°	3.31/3.38/2.19
B_{eq}/B_m, mp = south field line end	>15.1/17.4/14.5°	2.70/4.19/1.79

Constraints on equatorial pitch angles.
Column 1: mp = mirror point, λ_m = last part of Eq. 3 and B_{eq}/B_m = middle part.
Column 2: Average on all/northern/southern points ($N_{samples}$=36/7/29).
Column 3: Std. deviation (all/northern/southern points).

rial pitch angles could help constrain the radiation models of Jupiter. Using the equations valid in a dipole the equatorial pitch angle can be found as (Baumjohan & Treumann, 2012, Chap. 3):

$$\sin^2(\alpha_{eq}) = \frac{B_{eq}}{B_m} = \frac{\cos^6 \lambda_m}{(1 + 3\sin^2 \lambda_m)^{0.5}} \ , \tag{3}$$

where α_{eq} is the equatorial pitch angle, B_{eq} the equatorial field strength, B_m the field strength at the mirror point, and λ_m the magnetic latitude of the mirror point. For our use of the equation we take B_{eq} to be the equatorial field strength of the field line that intersects with the location of the detections we investigate.

If the particles are indeed trapped then the location of detection is the minimum latitude for the mirror point and inserting that into the last part of Eq. 3 gives the maximum equatorial pitch angle as any particle with a higher pitch angle would bounce back before reaching that point. Using the middle and last part of the equation yields slightly different estimates, the results of which are shown in Tab. 1. Results using all points below 1.6 R_J (except the detection at 24S, 106E) are shown as well as results for looking at detections north and south of the equator separately.

Using the location where the field lines that Juno intersects during the detections (as seen in Fig. 4) hit the atmosphere of Jupiter, we can estimate a minimum equatorial pitch angle - if it was smaller than this value the particle would not bounce back before entering the atmosphere. This gives four different values, using either the northern or southern termination of the field lines with either the middle or last part of Eq. 3. Using the lowest calculated value of the minimum angle and the highest value for the maximum angle we suggest a range of equatorial pitch angles between 10.1 and 27.1°. Roussos et al. (2022) calculates Pitch Angle Distributions (PADs) based on the Galileo heavy ion detections. For 3 of their 4 energy bands (5-46 MeV/nucleon for oxygen and 7-70 MeV/nucleon for sulfur) the calculated PADs peak around 90°, however their most energetic band (>50/70 MeV/nucleon for oxygen and sulfur respectively, shows a minimum around 90° near the Amalthean ring where the observations reported here are also found. Instead the PADs here peak at angles <30° (and >150°) in good correspondence with the results presented in this work which are also found in this location and at high energies.
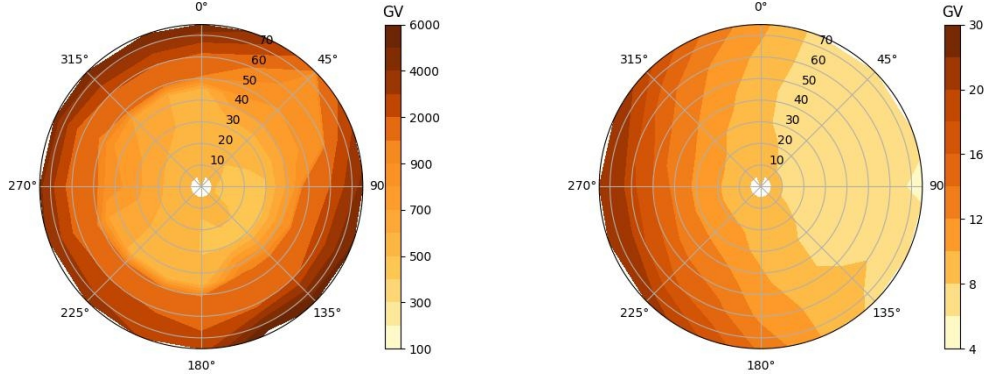
Figure 5: Skyview cutoff rigidity maps (in GV) at a: 1.41 R$_J$, 34.3^{o}S, 52.99^{o}E and b: 15.2 R$_J$, 2.42^{o}S, 322.14^{o}E (S3RH) for different angles of approach. Azimuthal angles follow the circumference of the circle while zenith angles follow the radius. The resolution is 1 GV for cutoff rigidity, 20-25 degrees for azimuth angles, 15 degrees for zenith angles, ending at 75° since the calculation of the trajectories start to fail at higher angles. 5° was added to provide more detail at lower zenith angles

.

4 Conclusion

A map of vertical cutoff rigidities has been calculated for Galactic Cosmic Ray entry into the atmosphere of Jupiter using the comprehensive JRM33 model of Jupiter's magnetic field along with modified Geomagnetic Cutoff Rigidity Computer Program particle trajectory code. The map was combined with measurements of the GCR proton flux at Earth (from BESS-Polar ii) to calculate a corresponding protron flux map at Jupiter. Additional cutoff rigidity maps were calculated for 1000 km above the 1 bar level, and at 1.41 R$_J$. These results could be useful for both design of future missions to Jupiter and to understand phenomena in the Jovian atmosphere.

Additionally, detections of heavy particles from Juno's SRU were analyzed for their cutoff rigidities in multiple directions. Cutoff rigidities of 3.5-8.5 GV were found for the five detections furthest out making them possible GCR candidates. The majority of points, located below 1.6 R$_J$ are not likely to be GCR. Assuming instead that they are trapped particles we have calculated upper and lower limits on their equatorial pitch angles, resulting in a range from 10.1° to 27.1°. These estimations can help constrain the models of Jupiter's radiation belts.

5 Open Research

SRU image data from PJs 22-35 supporting this study are provided in the Supporting information and at Zenodo (Becker et al., 2023). SRU Image data from orbits 36-42 are available from the Daubar et al. (2023). All figures were produced using Matplotlib for Python (Hunter, 2007), except for Fig. 1 which was made in Microsoft Excel 2016. Juno trajectory data as used in Fig. 4 can be from the J. Connerney (2022) and data used for the magnetic field lines and detection locations are in the Supporting information and at Zenodo (Enghoff et al., 2024). The planetary magnetic fields used in the plots were calculated with the wrldmagm program (MathWorks, 2023) for MATLAB R2022a, modified with the relevant planetary radii and magnetic field data input from the JRM33 model. The Geomagnetic Cutoff Rigidity Computer Program is written in full in Smart and Shea (2001) and our changes to the code are summarized in Tab. A1.

Table A1: Parameters changed in the Geomagnetic Cutoff Rigidity Computer Program

Name	New value
RHT	67.5 km
ISALT	67.5 km
R100km	337.5 km
R120km	405 km
ERAD	69911.0km
ERPLSQ	4469457316.0[a]
EREQSQ	5111106064.0[b]
DISOUT	80
DISCK	79.999[c]
FSTEP	4.0e09
LIMIT	6000000

[a]With the polar radius = 66854.0 km.
[b]With the equatorial radius = 71492 km.
[c]Only in the line IF (DISCK.GET:DISOUT)
THEN DISCK = 9.999.

Appendix A Changed model parameters

Tab. A1 shows what parameters in Geomagnetic Cutoff Rigidity Computer Program were changed for the simulations in Sect. 3.1. For the simulations at 1000 km and for the heavy ion detections the altitude parameters were changed accordingly.

Appendix B Map at 1000 km

Here in Fig. B1 we show the vertical cutoff rigidity similar to Fig. 2 (left) with the altitude for entry set to 1000 km instead of 67.5.

References

Abe, K., Fuke, H., Haino, S., Hams, T., Hasegawa, M., Horikoshi, A., . . . Yoshimura, K.   (2016, May 10).   Measurements of cosmic-ray proton and Helium spectry from the Bess-Polar long-duration balloon flights over Antarctica. *Astrophysical Journal*, *822*(2). doi: 10.3847/0004-637X/822/2/65

Alken, P., Thebault, E., Beggan, C. D., Amit, H., Aubert, J., Baerenzung, J., . . . Zhou, B.   (2021, Feb 11).   International Geomagnetic Reference Field: the thirteenth generation.   *Earth Planets and Space*, *73*(1).   doi: 10.1186/s40623-020-01288-x

Baumjohan, W., & Treumann, R. A.   (2012).   *Basic space plasma physics*.   London: Imperial College Press.

Becker, H. N., Alexander, J. W., Adriani, A., Mura, A., Cicchetti, A., Noschese, R., . . . Selex Galileo Juno SRU Team   (2017, Nov).   The Juno Radiation Mon-
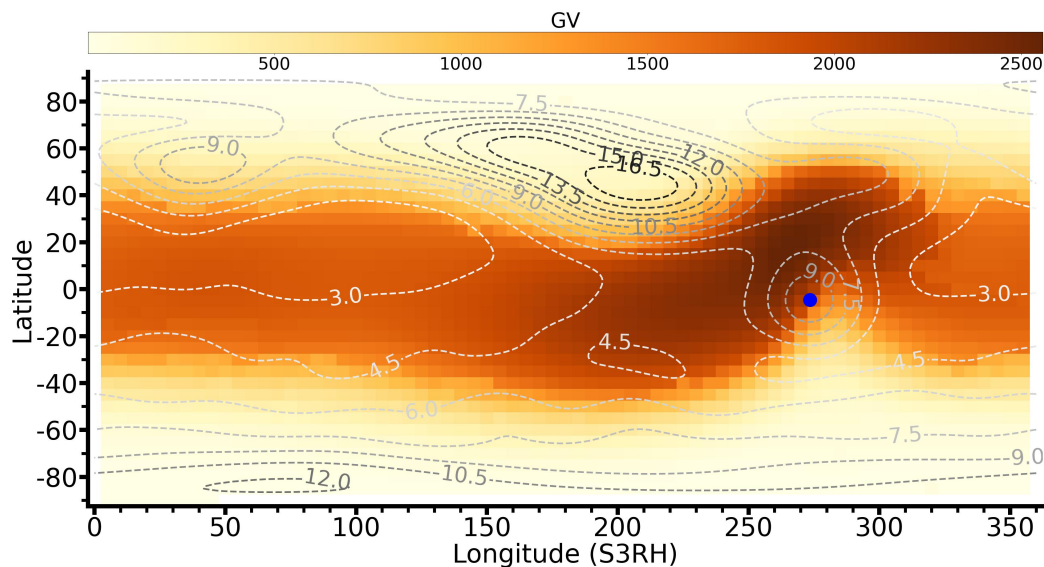
Figure B1: The cutoff rigidity map (in GV) of Jupiter at 5x5 degree spatial resolution 1000 km above the 1 bar line. The total intensity of the magnetic field is overplotted as coloured contour lines. Both the magnetic field and rigidities are calculated using 12 orders and degrees of Legendre functions.

itoring (RM) Investigation. *Space Science Reviews*, *213*(1-4), 507-545. doi: 10.1007/s11214-017-0345-9

Becker, H. N., Alexander, J. W., Connerney, J. E. P., Brennan, M. J., Guillaume, A., Adumitroaie, V., ... Bolton, S. J. (2021). High Latitude Zones of GeV Heavy Ions at the Inner Edge of Jupiter's Relativistic Electron Belt. *Journal of Geophysical Research: Planets*, *126*(5), e2020JE006772. Retrieved from https://agupubs.onlinelibrary.wiley.com/doi/abs/10.1029/2020JE006772 (e2020JE006772 2020JE006772) doi: https://doi.org/10.1029/2020JE006772

Becker, H. N., Alexander, J. W., Florence, M. M., Brennan, M. J., & Adumitroaie, V. (2023). *Juno Stellar Reference Unit (SRU) image data for high energy ion detections during perijoves 22-35.* Retrieved from https://zenodo.org/records/8256413 doi: 10.5281/zenodo.8256413

Bolton, S., Janssen, M., Thorne, R., Levin, S., Klein, M., Gulkis, S., ... West, R. (2002, Feb 28). Ultra-relativistic electrons in Jupiter's radiation belts. *Nature*, *415*(6875), 987-991. doi: 10.1038/415987a

Bolton, S., Levin, S., Gulkis, S., Klein, M., Sault, R., Bhattacharya, B., ... Leblanc, Y. (2001, Mar 1). Divine-Garrett model and Jovian synchrotron emission. *Geophysical Research Letters*, *28*(5), 907-910. doi: 10.1029/2000GL012071

Bolton, S. J., Lunine, J., Stevenson, D., Connerney, J. E. P., Levin, S., Owen, T. C., ... Thorpe, R. (2017, Nov). The Juno Mission. *Space Science Reviews*, *213*(1-4), 5-37. doi: 10.1007/s11214-017-0429-6

Bray, J., & Nelles, A. (2016). Minimal Prospects for Radio Detection of Extensive Air Showers in the Atmosphere of Jupiter. *The Astrophysical Journal*, *825*. doi: 10.3847/0004-637X/825/2/129

Breitschwerdt, D., Feige, J., Shulreich, M., Avillez, M. d., Dettbarn, C., & Fuchs, B. (2016). The locations of recent supernovae near the Sun from modelling 60Fe transport. *Nature*, *532*, 73–76. doi: 10.1038/nature17424

Burke, BF and Franklin, KL, T. . O. (1955). *Journal of Geophysical Research*, *60*(2), 213-217. doi: 10.1029/JZ060i002p00213

Caballero-Lopez, R., & Moraal, H. (2004, Jan 2). Limitations of the force field equation to describe cosmic ray modulation. *Journal of Geophysical Research - Space Physics*, *109*(A1). doi: 10.1029/2003JA010098

Connerney, J. (2015). 10.06 - planetary magnetism. In G. Schubert (Ed.), *Treatise on Geophysics (Second Edition)* (Second Edition ed., p. 195-237). Oxford: Elsevier. Retrieved from https://www.sciencedirect.com/science/article/pii/B9780444538024001718 doi: https://doi.org/10.1016/B978-0-444-53802-4.00171-8

Connerney, J. (2022). *Juno MAG calibrated data J V1.0, JNO-J-3-FGM-CAL-V1.0, NASA Planetary Data System.* NASA Planetary Data System. doi: https://doi.org/10.17189/1519711

Connerney, J. E. P., Acuña, M. H., Ness, N. F., & Satoh, T. (1998). New models of Jupiter's magnetic field constrained by the Io flux tube footprint. *Journal of Geophysical Research: Space Physics*, *103*(A6), 11929-11939. Retrieved from https://agupubs.onlinelibrary.wiley.com/doi/abs/10.1029/97JA03726 doi: https://doi.org/10.1029/97JA03726

Connerney, J. E. P., Benn, M., Bjarno, J. B., Denver, T., Espley, J., Jorgensen, J. L., . . . Smith, E. J. (2017, Nov). The Juno Magnetic Field Investigation. *Space Science Reviews*, *213*(1-4), 39-138. doi: 10.1007/s11214-017-0334-z

Connerney, J. E. P., Timmins, S., Oliversen, R. J., Espley, J. R., Joergensen, J. L., Kotsiaros, S., . . . Levin, S. M. (2022, Feb). A New Model of Jupiter's Magnetic Field at the Completion of Juno's Prime Mission. *Journal of Geophysical Research - Planets*, *127*(2). doi: 10.1029/2021JE007055

Cooper, J. F., & Simpson, J. A. (1980). Sources of high-energy protons in Saturn's magnetosphere. *Journal of Geophysical Research: Space Physics*, *85*(A11), 5793-5802. doi: https://doi.org/10.1029/JA085iA11p05793

Daubar, I., et al. (2023). *Juno SRU EDR V1.0, NASA Planetary Data System, JUNO-J-SRU-EDR-2-L0-V1.0 .* doi: https://doi.org/10.17189/e1kz-jt85

Enghoff, M. B., Pedersen, J. O. P., Bondo, T., Johnson, M. S., Paling, S., & Svensmark, H. (2008, Oct 16). Evidence for the Role of Ions in Aerosol Nucleation. *Journal of Physical Chemistry A*, *112*(41), 10305-10309. doi: 10.1021/jp806852d

Enghoff, M. B., Svensmark, J., Becker, H. N., Jørgensen, J. L., Kotsiaros, S., Herceg, M., . . . Connerney, J. E. P. (2024). *Data for Cutoff rigidities, galactic cosmic ray flux, and heavy ion detections at Jupiter.* Retrieved from https://zenodo.org/records/10513449 doi: 10.5281/zenodo.10513449

Fischer, H. M., Pehlke, E., Wibberenz, G., Lanzerotti, L. J., & Mihalov, J. D. (1996). High-Energy Charged Particles in the Innermost Jovian Magnetosphere. *Science*, *272*(5263), 856-858. Retrieved from https://www.science.org/doi/abs/10.1126/science.272.5263.856 doi: 10.1126/science.272.5263.856

Giesler, J., & Heber, B. (2016). Spatial gradients of GCR protons in the inner heliosphere derived from Ulysses COSPIN/KET and PAMELA measurements. *Astronomy & and Astrophysics*, *589*(A32). doi: 10.1051/0004-6361/201527972

Hess, S. L. G., Bonfond, B., Zarka, P., & Grodent, D. (2011). Model of the Jovian magnetic field topology constrained by the Io auroral emissions. *Journal of Geophysical Research: Space Physics*, *116*(A5). Retrieved from https://agupubs.onlinelibrary.wiley.com/doi/abs/10.1029/2010JA016262 doi: https://doi.org/10.1029/2010JA016262

Honig, T., Witasse, O. G., Evans, H., Nieminen, P., Kuulkers, E., Taylor, M. G. G. T., . . . Sánchez-Cano, B. (2019). Multi-point galactic cosmic ray measurements between 1 and 4.5 AU over a full solar cycle. *Annales Geo-*

physicae, *37*(5), 903–918. Retrieved from https://angeo.copernicus.org/articles/37/903/2019/ doi: 10.5194/angeo-37-903-2019

Hulsman, J., Wu, X., Azzarello, P., et al. (2023). Relativistic particle measurement in jupiter's magnetosphere with Pix.PAN. *Exp Astron*, *56*, 371-402. doi: https://doi.org/10.1007/s10686-023-09918-4

Hunter, J. D. (2007). Matplotlib: A 2D graphics environment. *Computing in Science & Engineering*, *9*(3), 90–95. doi: 10.1109/MCSE.2007.55

Levin, S., Bolton, S., Gulkis, S., & Klein, M. (2001). Modelling Jupiter's syncrhotron radiation. *Journal of Geophysical Research*, *28*(5), 903-906. doi: 10.1029/2000GL012087

Lockwood, J., & Webber, W. (1984). Integral Radial Cosmic-Ray Gradients in the Solar-System from 1972 to 1982. *Astrophysical Journal*, *279*(1), 151-156. doi: 10.1086/161875

Lockwood, J., & Webber, W. (1996). Comparison of the rigidity dependence of the 11-year solar cosmic ray variation at the earth in two solar cycles of opposite magnetic polarity. *Journal of Geophysical Research*, *101*(A10), 21573–21580.

Lovejoy, E. R., Curtius, J., & Froyd, K. D. (2004, Apr). Atmospheric ion-induced nucleation of sulfuric acid and water. *Journal of Geophysical Research (Atmospheres)*, *109*(D08204), 1-11. doi: 10.1029/2003JD004460

Lundstedt, H., Liszka, L., Lundin, R., & Muscheler, R. (2006). Long-term solar activity explored with wavelet methods. *Annales Geophysicae*, *24*(2), 769-778. doi: 10.5194/angeo-24-769-2006

MathWorks. (2023). *wrldmagm*. https://se.mathworks.com/help/aerotbx/ug/wrldmagm.html#bqsls45-1_vh.

Mauk, B. H., Haggerty, D. K., Jaskulek, S. E., Schlemm, C. E., Brown, L. E., Cooper, S. A., ... Stokes, M. R. (2017, November). The Jupiter Energetic Particle Detector Instrument (JEDI) Investigation for the Juno Mission. *Space Science Reviews*, *213*(1-4), 289-346. doi: 10.1007/s11214-013-0025-3

McComas, D. J., Alexander, N., Allegrini, F., Bagenal, F., Beebe, C., Clark, G., ... White, D. (2017, November). The Jovian Auroral Distributions Experiment (JADE) on the Juno Mission to Jupiter. *Space Science Reviews*, *213*(1-4), 547-643. doi: 10.1007/s11214-013-9990-9

Meitzler, R., Jun, I., Blse, R., et al. (2023). Investigating Europa's Radiation Environment with the Europa Clipper Radiation Monitor. *Space Sci Rev*, *219*(61). doi: https://doi.org/10.1007/s11214-023-01003-8

Mertens, C. J., Kress, B. T., Wiltberger, M., Tobiska, W. K., Grajewski, B., & Xu, X. (2012). Atmospheric Ionizing Radiation from Galactic and Solar Cosmic Rays. In M. Nenoi (Ed.), *Current topics in ionizing radiation research* (chap. 31). Rijeka: IntechOpen. Retrieved from https://doi.org/10.5772/32664 doi: 10.5772/32664

Moeckel, C., Janssen, M., & de Pater, I. (2019). A re-analysis of the Jovian radio emission as seen by Cassini-RADAR and evidence for time variability. *ICARUS*, *321*, 994-1012. doi: 10.1016/j.icarus.2018.12.013

Moore, K., Yadav, R., Kulowski, L., Cao, H., Bloxham, J., Connerney, J., ... Levin, S. (2018). A complex dynamo inferred from the hemispheric dichotomy of Jupiter's magnetic field. *Nature*, *561*, 76-78. doi: 10.1038/s41586-018-0468-5

Nénon, Q., Sicard, A., & Bourdarie, S. (2017). A new physical model of the electron radiation belts of Jupiter inside Europa's orbit. *Journal of Geophysical Research: Space Physics*, *122*, 5148-5167. doi: 10.1002/2017JA023893

Owens, M., Lang, M., Riley, P., Lockwood, M., & Lawless, A. (2020). Quantifying the latitudinal representivity of in situ solar wind observations. *J. Space Weather Space Clim.*, *10*(8). doi: 10.1051/swsc/2020009

Patrignani, C., Agashe, K., Aielli, G., Amsler, C., Antonelli, M., Asner, D. M., ... Grp, P. D. (2016, Oct). REVIEW OF PARTICLE PHYSICS Particle Data Group. *Chinese Physics C*, *40*(10). doi: 10.1088/1674-1137/40/10/100001

Piazzoli, B. D., Liu, S.-M., della Volpe, D., Cao, Z., Chiavassa, A., Piazzoli, B. D., ... Zhu, H. (2022, Mar). Chapter 4 Cosmic-Ray Physics *. *Chinese Physics C*, *46*(3), 030004. Retrieved from `https://dx.doi.org/10.1088/1674-1137/ac3faa` doi: 10.1088/1674-1137/ac3faa

Pinto, M., Gonçalves, P., Socha, P., Hajdas, W., Marques, A., & Costa Pinto, J. (2020). Beam test results of the RADEM Engineering Model. *Nuclear Instruments and Methods in Physics Research Section A: Accelerators, Spectrometers, Detectors and Associated Equipment*, *958*, 162795. Retrieved from `https://www.sciencedirect.com/science/article/pii/S0168900219312409` (Proceedings of the Vienna Conference on Instrumentation 2019) doi: https://doi.org/10.1016/j.nima.2019.162795

Pyle, K. R., McKibben, R. B., & Simpson, J. A. (1983). Pioneer 11 observations of trapped particle absorption by the Jovian ring and the satellites 1979, J1, J2, and J3. *Journal of Geophysical Research: Space Physics*, *88*(A1), 45-48. Retrieved from `https://agupubs.onlinelibrary.wiley.com/doi/abs/10.1029/JA088iA01p00045` doi: https://doi.org/10.1029/JA088iA01p00045

Ridley, V. A., & Holme, R. (2016). Modeling the Jovian magnetic field and its secular variation using all available magnetic field observations. *Journal of Geophysical Research: Planets*, *121*(3), 309-337. Retrieved from `https://agupubs.onlinelibrary.wiley.com/doi/abs/10.1002/2015JE004951` doi: https://doi.org/10.1002/2015JE004951

Rimmer, P., Stark, C., & Helling, C. (2014). Jupiter as a Giant Cosmic Ray Detector. *The Astrophysical Journal*, *787*. doi: 10.1088/2041-8205/787/2/L25

Roberts, J. (1976). The Pitch Angles of Electrons in Jupiter's Radiation Belt. *Proc. ASA*, *3*(1), 53-55. doi: 10.1017/S1323358000014636

Romani, P. N., Jennings, D. E., Bjoraker, G. L., Sada, P. V., McCabe, G. H., & Boyle, R. J. (2008, Dec). Temporally varying ethylene emission on Jupiter. *Icarus*, *198*(2), 420-434. doi: 10.1016/j.icarus.2008.05.027

Roussos, E., Allanson, O., Andre, N., Bertucci, B., Branduardi-Raymont, G., Clark, G., ... Yao, Z. (2021). The in-situ exploration of Jupiter's radiation belts. *Experimental Astronomy*. doi: 10.1007/s10686-021-09801-0

Roussos, E., Cohen, C., Kollmann, P., Pinto, M., Krupp, N., Gonçalves, P., & Dialynas, K. (2022). A source of very energetic oxygen located in Jupiter's inner radiation belts. *Science Advances*, *8*(2), eabm4234. Retrieved from `https://www.science.org/doi/abs/10.1126/sciadv.abm4234` doi: 10.1126/sciadv.abm4234

Roussos, E., Dialynas, K., Krupp, N., Kollmann, P., Paranicas, C., Roelof, E. C., ... Krimigis, S. M. (2020, Dec). Long- and Short-term Variability of Galactic Cosmic-Ray Radial Intensity Gradients between 1 and 9.5 au: Observations by Cassini, BESS, BESS-Polar, PAMELA, and AMS-02. *The Astrophysical Journal*, *904*(2), 165. Retrieved from `https://dx.doi.org/10.3847/1538-4357/abc346` doi: 10.3847/1538-4357/abc346

Santos-Costa, D., & Bolton, S. J. (2008, Mar). Discussing the processes constraining the Jovian synchrotron radio emission's features. *Planetary and Space Science*, *56*(3-4), 326-345. doi: 10.1016/j.pss.2007.09.008

Selesnick, R. (2002). Cosmic ray access to Jupiter's magnetosphere. *Geophysical Research Letters*, *29*, 1298. doi: 10.1029/2001GL014146

Shaviv, N. (2002). Cosmic Ray Diffusion from the Galactic Spiral Arms, Iron Meteorites, and a Possible Climatic Connection. *Physical Review Letters*, *89*(5), 051102-1–051102-4. doi: 10.1103/PhysRevLett.89.051102

Smart, D., & Shea, M. (1994). Geomagnetic cutoffs: A review for space dosimetry applications. *Adv. Space Res.*, *14*(10), 10787-10796.

Smart, D., & Shea, M. (2001). *Geomagnetic Cutoff Rigidity Computer Program: Theory, Software Description and Example* (Tech. Rep. No. 20010071975). Huntsville: University of Alabama Huntsville.

Smart, D., & Shea, M. (2005). A review of geomagnetic cutoff rigidities for earth-orbiting spacecraft. *Advances in Space Research*, *36*(10), 2012-2020. Retrieved from https://www.sciencedirect.com/science/article/pii/S0273117705001997 (Solar Wind-Magnetosphere-Ionosphere Dynamics and Radiation Models) doi: https://doi.org/10.1016/j.asr.2004.09.015

Smart, D., Sheas, M., Tylka, A., & Boberg, P. (2006). A geomagnetic cutoff rigidity interpolation tool: Accuracy verification and application to space weather. *Advance in Space Research*, *37*, 1206-1217.

Svensmark, H., Enghoff, M. B., & Pedersen, J. O. P. (2013). Response of cloud condensation nuclei (¿50 nm) to changes in ion-nucleation. *Physics Letters A*, *377*(37), 2343 - 2347. Retrieved from http://www.sciencedirect.com/science/article/pii/S0375960113006294 doi: http://dx.doi.org/10.1016/j.physleta.2013.07.004

Svensmark, H., Svensmark, J., Enghoff, M. B., & Shaviv, N. J. (2021, Oct 11). Atmospheric ionization and cloud radiative forcing. *Scientific Reports*, *11*(1). doi: 10.1038/s41598-021-99033-1

Usoskin, I., & Kovaltsov, G. (2006). Cosmic ray induced ionization in the atmosphere: Full modeling and practical applications. *Journal of Geophysical Research*, *111*(D21206). doi: 10.1029/2006JD007150

Vargas, B., & Valdés-Galicia, J. (2011). Calculation of the magnetic rigidity cutoff and the asymptotic cone of acceptance for the site of the Pierre Auger Observatory in Malargue, Argentina. *32nd International Cosmic Ray Conference, Beijing*, *10*, 249-251. doi: 10.7529/ICRC2011/V10/1099